Flexible Hexagon, an approach to utilize distributed module voltages to reduce voltage-time area errors of multilevel converters

1st Tobias Merz
Elektrotechnisches Institut (ETI)
Karlsruhe Institute of Technology (KIT)
Karlsruhe, Germany
tobias.merz@kit.edu

2nd Nikolas Menger
Elektrotechnisches Institut (ETI)
Karlsruhe Institute of Technology (KIT)
Karlsruhe, Germany

3rd Hannah Graute
Elektrotechnisches Institut (ETI)
Karlsruhe Institute of Technology (KIT)
Karlsruhe, Germany

4th David Kraus
Institut für Technik der Informationsverarbeitung (ITIV)
Karlsruhe Institute of Technology (KIT)
Karlsruhe, Germany

5th Rüdiger Schwendemann
Elektrotechnisches Institut (ETI)
Karlsruhe Institute of Technology (KIT)
Karlsruhe, Germany

6th Marc Hiller
Elektrotechnisches Institut (ETI)
Karlsruhe Institute of Technology (KIT)
Karlsruhe, Germany

***Abstract*—In this paper, a new approach to utilize varying module voltages in multilevel converters (MC) is presented. By actively distributing the module voltages within a defined range, additional intermediate switching levels become available. Using these enables output voltages with lower voltage-time area errors (VTAE) and therefore output currents with reduced ripple without requiring a higher switching frequency or larger filter components. Since the proposed modulation method adds module voltage dependent and thus, flexible, additional sub-triangles in the $\alpha\beta$-plane, it is referred to as Flexible-Hexagon Modulation. Calculation results demonstrate that improved module voltage distributions can reduce the mean VTAE compared to an MC with equal module voltages across a wide operating range by about 50%.**

***Index Terms*—Voltage-Time Area Error, Space Vector Modulation, Multilevel Converter, Cascaded H-Bridge**

I. Introduction

In 1969, the first Cascaded H-Bridge (CHB) multilevel converter was introduced [1]. Later, additional multilevel topologies such as the Neutral Point Clamped (NPC) and the Flying-Capacitor (FC) converters were proposed [2], [3]. In 2003, the Modular Multilevel Converter (MMC) was presented [4]. All of these multilevel topologies share a common feature: the voltage difference between two adjacent switching levels of a single phase is equal. As a result, applying Clarke's transformation to all valid switching states produces a symmetrical hexagon in the $\alpha\beta$-plane. The required phase-to-phase voltages can be synthesized by various switching states inside this hexagon. However, multiple physical switching states can realize the same output voltage. Typically, these redundant switching options are exploited to minimize switching transitions and to balance both the capacitor voltages and the module temperatures [1]. Depending on the topology and application, however, voltage and temperature balancing can also be achieved without relying on switching state redundancy [5].

While new converter topologies were developed, modulation schemes were also the focus of intensive research. The first publication on Space Vector Modulation (SVM) appeared in [6], followed by improvements in [7], [8]. A survey of various pulse-width modulation techniques and their performance criteria is presented in [9]. In contrast to fixed-frequency schemes, indirect modulation approaches such as model predictive control have been proposed to reduce current ripple without increasing the switching frequency [10]–[12]. However, their main drawback is that high model accuracy and sub-millisecond evaluation are necessary to achieve superior results, which requires significant computational effort [13].

In this paper, an enhancement of standard fixed-frequency SVM is proposed. The strict constraint of equal module voltages in multilevel converters is relaxed in favor of an actively controlled voltage distribution among the modules. Instead of assigning identical voltages to all sub-modules (SMs), a generalized SVM approach, referred to as Flexible Hexagon Modulation (FlexHex), is introduced and analyzed. Unlike earlier works [14]–[16], which rely on specifically designed SMs to improve output voltage quality, the FlexHex method enables a more flexible and systematic utilization of available voltage levels using the same hardware. While equal or fixed module voltages represent one limiting case, the opposite extreme is shown in [17], where each SM voltage in a CHB converter is dynamically controlled to generate a continuous AC output voltage. FlexHex establishes a compromise between these extremes by allowing quasi-fixed, operating-point-dependent module voltages to improve the effective switching state density and, consequently, the output voltage quality.

TABLE I
Switching states of the CHB cell

State	Conducting/(Blocking) MOSFETs	Output voltage u_{FB}	Module current i_{mod}
Positive	$\mathrm{T}_1, \mathrm{T}_4$ / $(\mathrm{T}_2, \mathrm{T}_3)$	$+U_{\mathrm{mod}}$	i_{AC}
Negative	$\mathrm{T}_2, \mathrm{T}_3$ / $(\mathrm{T}_1, \mathrm{T}_4)$	$-U_{\mathrm{mod}}$	$-i_{\mathrm{AC}}$
Bypass 1	$\mathrm{T}_1, \mathrm{T}_3$ / $(\mathrm{T}_2, \mathrm{T}_4)$	0 V	0 A
Bypass 2	$\mathrm{T}_2, \mathrm{T}_4$ / $(\mathrm{T}_1, \mathrm{T}_3)$	0 V	0 A

II. Topology

All modular multilevel topologies with distributed DC links can utilize FlexHex, since two Degrees of Freedom (DoFs) are available to compose the output voltage. Usually, only one DoF is actively used by switching the CHB stage at the AC output through Pulse Width Modulation (PWM). However, the second DoF is modifying the module voltages U_{mod} instead of switching the CHB stage.

When using the standard MMC topology [4], a superimposed controller can be employed to adjust the module voltages to their respective setpoints. In CHB topologies, where there is a galvanically isolated power source for each SM, the voltage of each module can be controlled independently. In an MMC with distributed batteries, e.g. [18], the State of Charge (SoC) of each battery, and thus the corresponding module voltage, cannot be controlled directly and will naturally vary among the modules. This variation becomes more pronounced when second-life batteries are used, as done in [19]. Even with such uncontrolled module voltages, FlexHex can be applied to reduce both the Voltage-Time Area Error (VTAE) and, consequently, the harmonic distortion of the output current.

For simplicity, this paper focuses on an Solid-State Transformer (SST) topology in an input serial output parallel (ISOP) configuration in star connection, as illustrated in Fig. 1. Each phase x, with $x \in \{\mathrm{U}, \mathrm{V}, \mathrm{W}\}$, consists of a series connection of several SMs. Each SM is composed of a Dual Active Bridge (DAB) stage, which operates as a bidirectional DC/DC converter, and a CHB full-bridge cell, shown in blue and green, respectively. The left-hand (primary) side of the SST is supplied by a DC voltage source U_{p}. The CHB structure on the right-hand (secondary) side generates the AC output voltages $u_{\mathrm{AC},x}$ that drive the respective phase currents $i_{\mathrm{AC},x}$. These outputs are connected to the AC grid through the grid filter inductances L_{grid}.

Fig. 2 shows the structure of the SMs. The DAB, consisting of two full-bridges and the medium-frequency transformer (MFT) with winding ratio n_{t} and leakage inductance L_σ, actively controls the module voltage U_{mod}. The CHB cell (green) of each power module, consisting of four MOSFETs T_1 to T_4, provides three discrete voltage levels ($+U_{\mathrm{mod}}$, $-U_{\mathrm{mod}}$, or 0 V) depending on the switching state of the MOSFETs, as summarized in Table I.

III. Concept

Although multilevel converters offer finer voltage resolution than two-level converters, they still exhibit a VTAE $\Phi_{\mathrm{e}}(t)$ due to the limited number of discrete switching states and a constrained switching frequency f_{sw}. In combination with the filter stage, this VTAE causes ripple in the AC output current. Because of the inherent time and voltage discretization in conventional modulation techniques such as SVM, Space Vector Delta-Sigma Modulation [20], or phase-individual PWM, this ripple cannot be completely eliminated.

If the requirement for time discretization is removed, model predictive approaches can be applied to reduce the VTAE. In these methods, the instantaneous current deviation, which is comparable to the ripple, is a key factor for determining both the switching instant and the next switching state [12]. Removing the additional limitation of output discretization enables continuous output generation, which can be realized either by a purely linear amplifier, though at very low efficiency, or by a hybrid converter combining switched and linear stages. The latter offers medium efficiency and highly accurate, continuous output voltages, making it suitable for specialized applications such as emulation [21], [22].

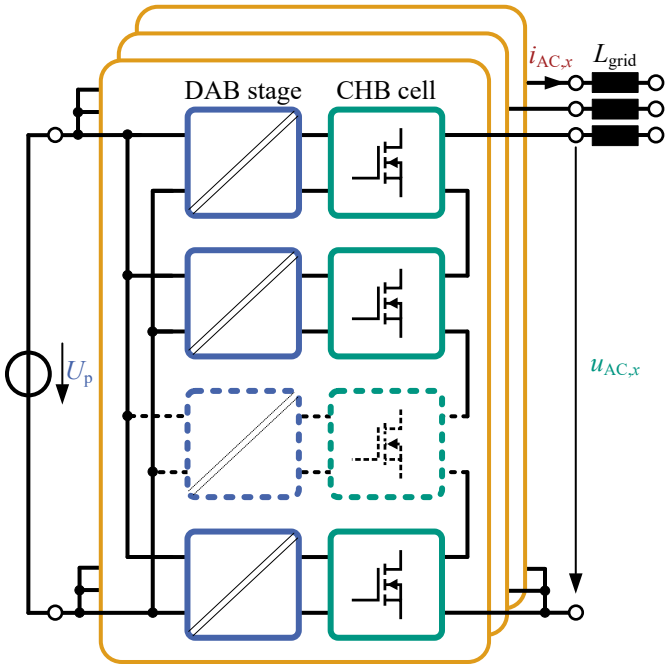

Fig. 1: Three phase modular ISOP SST. The dotted module means that there can be several modules.

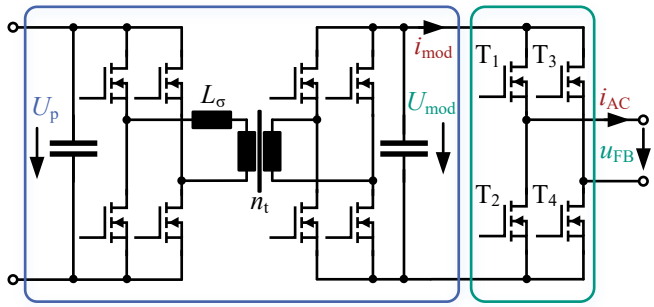

Fig. 2: SM with DAB stage for power supply (blue) and CHB cell output stage (green).

The key idea behind the proposed FlexHex method is to combine high efficiency switching with improved voltage level selection. The constraint of equal module voltages is relaxed to exploit the converter's internal DoFs by intentionally distributing the module voltages unevenly and quasi-stationary. This enables the generation of additional intermediate voltage levels, resulting in a "multi-multilevel" structure with enhanced output voltage granularity. By increasing the resolution of available output levels, the resulting VTAE during modulation, and thus the ripple in the output current, can be reduced without increasing the switching frequency or requiring more hardware components.

A. Amount of switching levels

Due to the CHB structure each phase has $S_{\mathrm{ph,th}} = 3^{m_{\mathrm{ph}}}$ possible unique switching combinations, where m_{ph} denotes the number of modules per phase. Although switching modules in opposing directions within the same phase can be beneficial for voltage synthesis [14]–[17], this option is excluded for FlexHex due to its increase in complexity and increased circulating power. As a result, a total of $S_{\mathrm{ph}} = 2 \cdot 2^{m_{\mathrm{ph}}} - 1 = 2^{m_{\mathrm{ph}}+1} - 1$ valid switching states per phase are further considered.

In converters with equal module voltages U_{mod}, the same AC output voltage $u_{\mathrm{AC},x}$ for phase x can be synthesized by different physical switching states, except at the maximum voltage levels, which have only one possible switching state representation. Consequently, evaluating the number of unique output voltage levels per phase leads to $L_{\mathrm{ph,eq}} = 2m_{\mathrm{ph}} + 1$.

From this it follows that the total number of physical switching states of the entire three-phase converter, S_{conv}, can be calculated using (1). To determine the total number of unique output voltage levels under the constraint of equal module voltages, $L_{\mathrm{conv,eq}}$, (2) is used. A comparison of these equations clearly shows a significant reduction in available output voltage levels when equal module voltages are enforced.

$$S_{\mathrm{conv}} = S_{\mathrm{ph}}^3 = (2^{m_{\mathrm{ph}}+1} - 1)^3 \tag{1}$$

$$L_{\mathrm{conv,eq}} = L_{\mathrm{ph,eq}}^3 = (2m_{\mathrm{ph}} + 1)^3 \tag{2}$$

To limit the number of distinct output voltage levels per phase to a practical value $L_{\mathrm{ph}} \ll S_{\mathrm{ph}}$, the SMs are grouped into $|M| = n$ equal voltage groups, with $M = \{m_1, m_2, ..., m_n\}$. Each group contains $m_i \in \mathbb{N}$ modules, with $i \in \{1, 2, ..., n\}$, and their sum equals the amount of modules per phase m_{ph}, c.f. (3). Their respective module voltages are $V = \{v_1, v_2, ..., v_n\}$. In general, grouping modules enables the usage of redundant switching states for load balancing.

$$m_{\mathrm{ph}} = \sum_{i=1}^{n} m_i \tag{3}$$

The resulting number of discrete output voltage levels per phase L_{ph} can be determined using (4). This holds if each output voltage level can only be generated by one unique switching combination of modules from the different voltage groups. This requirement can be expressed mathematically by (5).

$$L_{\mathrm{ph}} = 2 \cdot \left(\prod_{i=1}^{n} (m_i + 1) \right) - 1 \tag{4}$$

$$\sum_{i=1}^{n} \sigma_i d_i v_i = 0 \;\Rightarrow\; \sigma_i = 0 \;\forall i \tag{5}$$
$$\sigma_i \in \{1, 0, -1\},\; d_i \in \{1, 2, \ldots, m_i\}$$

Since some modules are not operated at their individual maximum voltage, the achievable output voltage of a single phase, $U_{\mathrm{AC,max}}$, is reduced accordingly. The maximum output voltage of a phase $U_{\mathrm{AC,max}}$ can be calculated using (6).

$$U_{\mathrm{AC,max}} = \sum_{i=1}^{n} m_i \cdot v_i \tag{6}$$

B. Generalized Space Vector Modulation

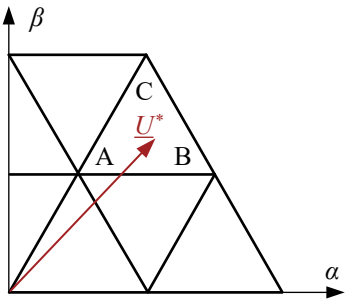

Fig. 3: First quadrant of a regular multilevel hexagon with three output levels per phase.

Fig. 3 illustrates the first quadrant of a multilevel hexagon in the $\alpha\beta$-plane with three output levels per phase. The vector $\underline{U}^*(t)$ represents the voltage setpoint as defined in (7). Depending on its position within the hexagon, the three switching states of the sub-triangle containing the setpoint are denoted as A, B, and C. Their positions in the $\alpha\beta$-plane can be described by (8), where $y \in \{\mathrm{A}, \mathrm{B}, \mathrm{C}\}$.

$$\underline{U}^* = U_\alpha^* + jU_\beta^* \tag{7}$$

$$\underline{U}_y = U_{\alpha,y} + jU_{\beta,y} \tag{8}$$

To calculate the switching state duration t_y, the system of linear equations (9)-(11) has to be solved. In this work, a two-arm SVM with a minimum number of switching transitions is employed. Accordingly, the order of switching states and their corresponding switching durations in parentheses is A $\left(\frac{t_{\mathrm{A}}}{2}\right)$ → B $\left(\frac{t_{\mathrm{B}}}{2}\right)$ → C (t_{C}) → B $\left(\frac{t_{\mathrm{B}}}{2}\right)$ → A $\left(\frac{t_{\mathrm{A}}}{2}\right)$. Nevertheless, application of the proposed method is also possible with three-arm PWM.

$$U_\alpha^* = \frac{t_{\mathrm{A}}}{T_{\mathrm{sw}}} U_{\alpha,\mathrm{A}} + \frac{t_{\mathrm{B}}}{T_{\mathrm{sw}}} U_{\alpha,\mathrm{B}} + \frac{t_{\mathrm{C}}}{T_{\mathrm{sw}}} U_{\alpha,\mathrm{C}} \tag{9}$$

$$U_\beta^* = \frac{t_{\mathrm{A}}}{T_{\mathrm{sw}}} U_{\beta,\mathrm{A}} + \frac{t_{\mathrm{B}}}{T_{\mathrm{sw}}} U_{\beta,\mathrm{B}} + \frac{t_{\mathrm{C}}}{T_{\mathrm{sw}}} U_{\beta,\mathrm{C}} \tag{10}$$

$$1 = \frac{t_{\mathrm{A}}}{T_{\mathrm{sw}}} + \frac{t_{\mathrm{B}}}{T_{\mathrm{sw}}} + \frac{t_{\mathrm{C}}}{T_{\mathrm{sw}}} \tag{11}$$

C. Evaluation of the VTAE

To compare the performance of different module voltage distributions (M, V) with respect to the resulting VTAE, the maximum of the Euclidean norm of the complex VTAE over one modulation cycle, $\Phi_{\mathrm{e,max}}$, is used as the evaluation criterion. It is calculated according to (12), with $\underline{\Phi}(t)$ defined in (13). The complex VTAE over time in the $\alpha\beta$-plane during modulation is determined using (14), where $\underline{U}(t)$ represents the complex voltage of the physical switching states (A, B and C). The modulation ensures that the geometric sum of the three voltage vectors of the selected switching states equals the setpoint vector. Consequently, the VTAE vanishes at the beginning, midpoint, and end of each switching period.

$$\Phi_{\mathrm{e,max}} = \max_t |\underline{\Phi}(t)| = \max_t \left(\sqrt{\Phi_\alpha^2(t) + \Phi_\beta^2(t)}\right) \tag{12}$$

$$\underline{\Phi}(t) = \Phi_\alpha(t) + j \cdot \Phi_\beta(t) \tag{13}$$

$$\underline{\Phi}(t) = \int_{0\,\mathrm{s}}^{t} (\underline{U}(\tau) - \underline{U}^*(\tau))\, \mathrm{d}\tau, \quad 0\,\mathrm{s} \le t \le T_{\mathrm{sw}} \tag{14}$$

$$\underline{\Phi}(t = 0\,\mathrm{s}) = \underline{\Phi}(t = \frac{T_{\mathrm{sw}}}{2}) = \underline{\Phi}(t = T_{\mathrm{sw}}) = 0\,\mathrm{Vs}$$

As mentioned above, for equal module voltages, the three switching states of the smallest sub-triangle within the hexagon that contains the setpoint vector $\underline{U}^*$ are used. In contrast, with distributed module voltages, multiple such triangles may exist. From this solution space, the sub-triangle that yields the minimum VTAE $\Phi_{\mathrm{e,max}}$ is selected.

D. Alternative Modulation Approach

If the constraint on minimum switching transitions is relaxed or another modulation scheme is desired, an extended Delta-Sigma Modulator (DSM) can be applied. This approach operates as a true nearest-level modulator in the $\alpha\beta$-plane. While a conventional DSM can be implemented as shown in [20], the Extended Delta-Sigma Modulator (EDM) dynamically selects the switching state of the "multi-multilevel" converter that is closest to the reference vector in terms of vector distance. As a result, the instantaneous VTAE is minimized at every sampling instant.

IV. Evaluation

This chapter presents the SST setup used for FlexHex and evaluates the resulting VTAE for various module voltage distributions. All calculations are performed using MATLAB.

A. System setup

For clarity and simplicity, only the first quadrant of the hexagon is analyzed. Due to system symmetries, the VTAE behavior in the remaining quadrants is equivalent. The evaluation considers $m_{\mathrm{ph}} = 4$ modules per phase, each with a nominal voltage of $U_{\mathrm{mod}} = 1000\,\mathrm{V}$. The modulation frequency is set to $f_{\mathrm{sw}} = 1/T_{\mathrm{sw}} = 10\,\mathrm{kHz}$.

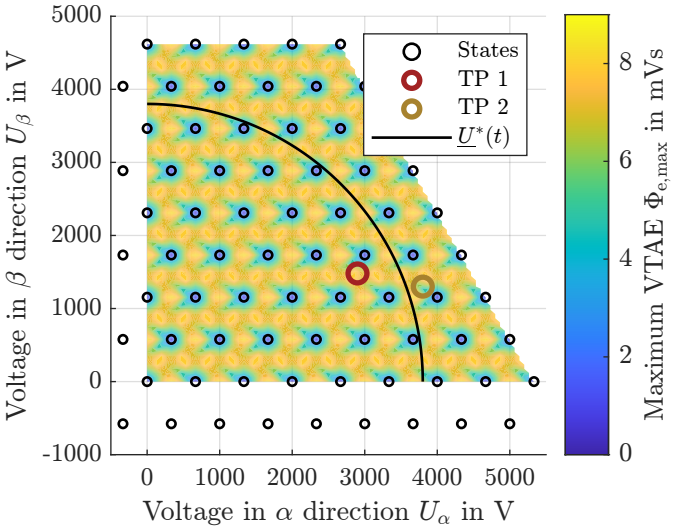

Fig. 4: Possible switching states with $L_{\mathrm{ph}} = 9$ and resulting maximum VTAE $\Phi_{\mathrm{e,max}}$ for $M = 4$, $V = 1000\,\mathrm{V}$, and two-arm SVM. The mean value of $\Phi_{\mathrm{e,max}}$ over the investigated operating range is $\overline{\Phi}_{\mathrm{e,max}} = 6.3\,\mathrm{mVs}$.

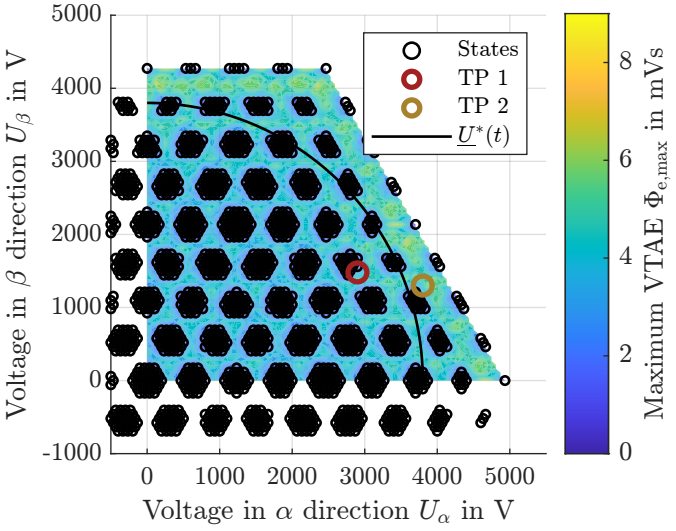

Fig. 5: Possible switching states and resulting maximum VTAE $\Phi_{\mathrm{e,max}}$ with $M = \{2, 1, 1\}$, $V = \{1000\,\mathrm{V}, 900\,\mathrm{V}, 800\,\mathrm{V}\}$. The mean value of maximum VTAE over the investigated operation range is $\overline{\Phi}_{\mathrm{e,max}} = 3.0\,\mathrm{mVs}$.

B. Calculated results

The resulting maximum VTAE $\Phi_{\mathrm{e,max}}$ for each setpoint in the $\alpha\beta$-plane for $M = 4$ and $V = 1000\,\mathrm{V}$, corresponding to $L_{\mathrm{ph}} = 9$ output voltage levels per phase, is shown in the colored background of Fig. 4. Black circles mark available switching states, and the black line illustrates an example setpoint voltage vector $\underline{U}^*(t)$ with a magnitude of $3800\,\mathrm{V}$. As expected, when the voltage setpoint is close to a switching state, the resulting VTAE in this modulation cycle approaches zero, whereas setpoints between adjacent switching states cause local peaks. Two exemplary Test points (TPs) highlighted in red and brown allow for a more detailed comparison.

In contrast to Fig. 4, Fig. 5 illustrates the resulting maximum VTAE for the distributed voltage set $M = \{2, 1, 1\}$

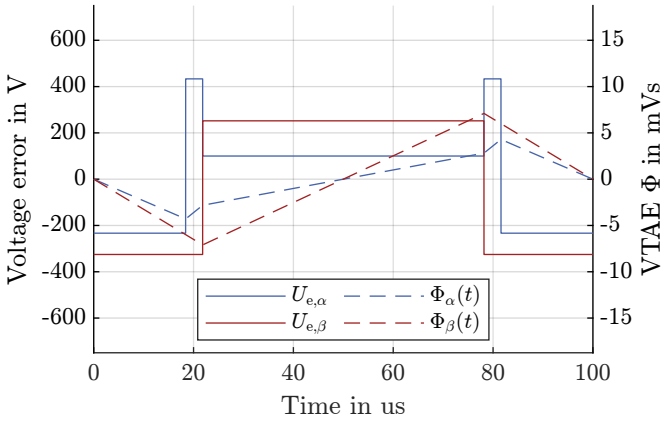

Fig. 6: Voltage errors and VTAE for TP 1 with $\Phi_{e,max} = 7.6\,\mathrm{mVs}$ and $(M = \{4\}, V = \{1000\,\mathrm{V}\})$.

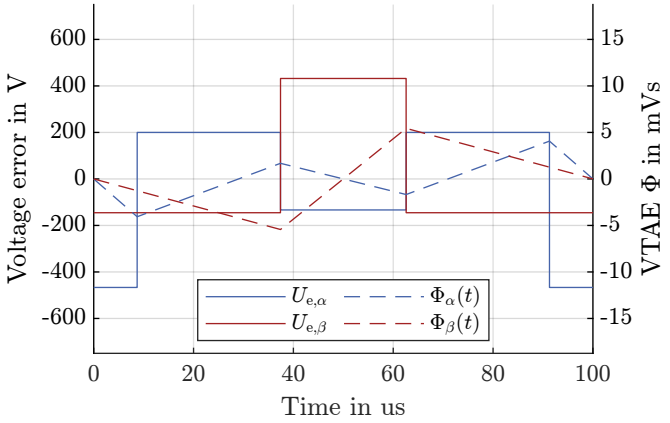

Fig. 7: Voltage errors and VTAE for TP 2 with $\Phi_{e,max} = 5.7\,\mathrm{mVs}$ and $(M = \{4\}, V = \{1000\,\mathrm{V}\})$.

and $V = \{1000\,\mathrm{V}, 900\,\mathrm{V}, 800\,\mathrm{V}\}$, yielding a total of $L_{ph} = 23$ output voltage levels per phase. The increased number of switching state combinations allows the setpoint vector to be approximated more accurately, resulting in a significantly lower $\Phi_{e,max}$ as indicated by the larger blue-shaded areas. However, due to the reduced module voltages, the maximum achievable output voltage is decreased.

To further highlight the VTAE for different module voltage sets, the time course of the voltage errors $U_{e,\alpha}(t) = U_\alpha(t) - U^*_\alpha(t)$ and $U_{e,\beta}(t) = U_\beta(t) - U^*_\beta(t)$, as well as the resulting VTAE in these directions, are illustrated in the time-domain. Fig. 6 and Fig. 7 show the values for TP 1 and TP 2, respectively, with $M = \{4\}$, $V = \{1000\,\mathrm{V}\}$. By applying distributed module voltages, the setpoint vector can be approximated more accurately, as shown in Fig. 8 and Fig. 9. Consequently, the maximum VTAE values decrease significantly: from $7.6\,\mathrm{mVs}$ to $3.3\,\mathrm{mVs}$ for TP 1, and from $5.7\,\mathrm{mVs}$ to $4.7\,\mathrm{mVs}$ for TP 2. Across the entire operating range, the mean maximum VTAE can be reduced by up to $50\,\%$, from $\overline{\Phi}_{e,max} = 6.3\,\mathrm{mVs}$ to $\overline{\Phi}_{e,max} = 3.0\,\mathrm{mVs}$.

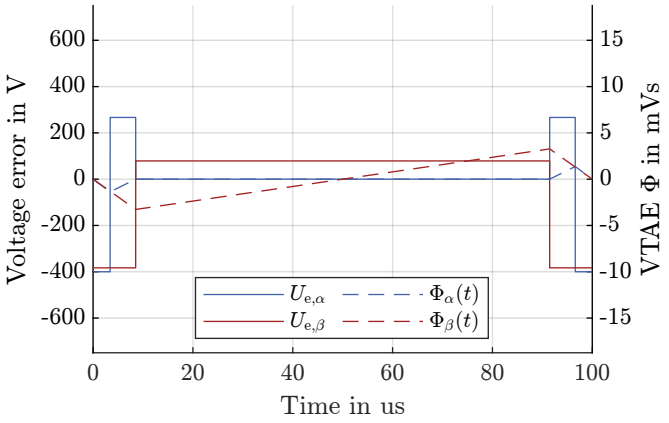

Fig. 8: Voltage errors and VTAE for TP 1 with $\Phi_{e,max} = 3.3\,\mathrm{mVs}$ and $(M = \{2, 1, 1\}, V = \{1000\,\mathrm{V}, 900\,\mathrm{V}, 800\,\mathrm{V}\})$.

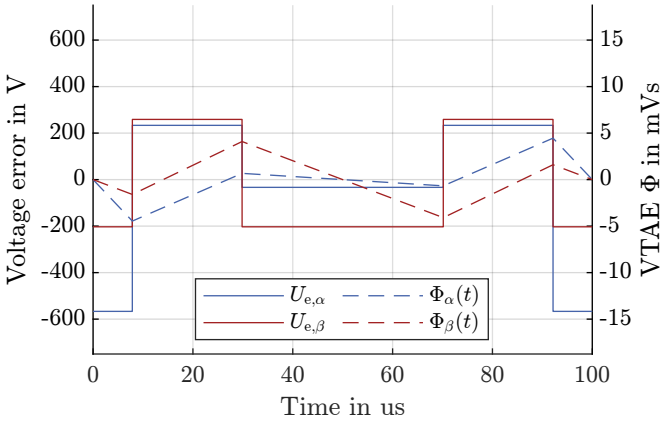

Fig. 9: Voltage errors and VTAE for TP 2 with $\Phi_{e,max} = 4.7\,\mathrm{mVs}$ and $(M = \{2, 1, 1\}, V = \{1000\,\mathrm{V}, 900\,\mathrm{V}, 800\,\mathrm{V}\})$.

C. Operation point dependent module voltage distribution

As shown for two specific operation points, distributed module voltages can effectively reduce the VTAE. Fig. 10 illustrates the maximum VTAE $\Phi_{e,max}$ during modulation in the first quadrant for different voltage setpoints $\underline{U}^*$ and various module voltage distributions (D1–D6). The vertical black lines indicates a voltage setpoint of $\underline{U}^* = 3800\,\mathrm{V}$ as illustrated in Fig. 4 and Fig. 5. Distribution D1, representing equal module voltages, results in the highest VTAE across the entire operating range. The lowest VTAE values are achieved with distribution D2 and D3, indicating that an appropriate voltage distribution can substantially improve modulation accuracy. However, while decreasing individual module voltages generally reduces the VTAE, it simultaneously lowers the maximum achievable output voltage. Consequently, a trade-off must be made between minimizing the VTAE and maintaining the required output voltage capability. The optimal distribution thus depends on the specific operating conditions and application requirements, and no universal optimum can be defined.

D. Line-to-Line voltages

Fig. 11 shows the example for the line-to-line voltages for two different module voltage distributions (D1:

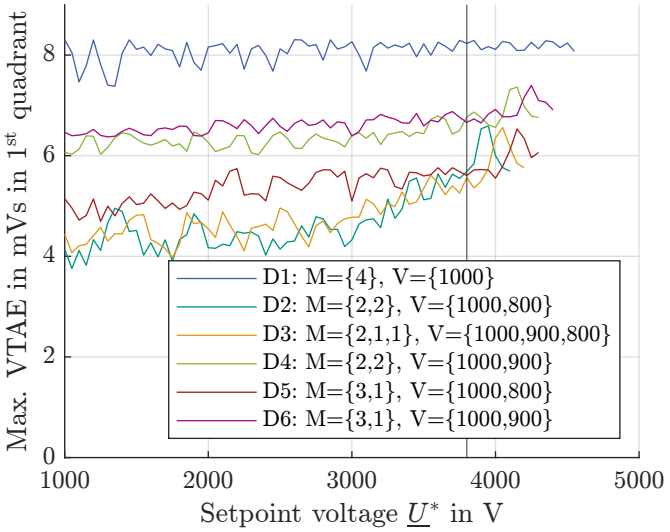

Fig. 10: Maximum VTAE $\Phi_{\mathrm{e,max}}$ for different setpoint voltages $\underline{U}^*$ and module voltage distributions M and V in the first quadrant of the $\alpha\beta$-plane. The black vertical line shows a setpoint voltage of $\underline{U}^* = 3800\,\mathrm{V}$.

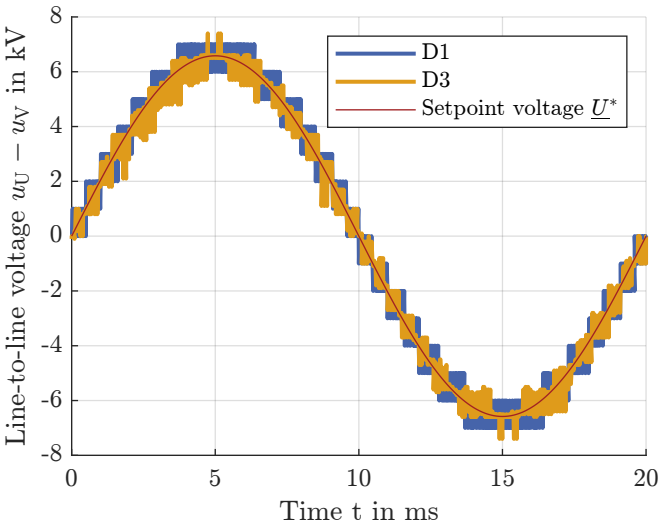

Fig. 11: Line-to-line voltages $u_\mathrm{U} - u_\mathrm{V}$ with different module voltage distributions D1 (blue), D3 (orange) and setpoint voltage (red).

$M = \{4\}$, $V = \{1000\}$ in blue and D3: $M = \{2,1,1\}$, $V = \{1000, 900, 800\}$ in orange) for a reference voltage of $\underline{U}^* = 3800\,\mathrm{V}$. This reference corresponds to a line-to-line voltage amplitude of $u_\mathrm{UV} = \sqrt{3} \cdot 3800\,\mathrm{V} \approx 6600\,\mathrm{V}$, indicated in red. Owing to the multi-multilevel structure of FlexHex, a larger number of intermediate voltage levels can be synthesized. As a result, the harmonic spectrum shown in Fig. 12 is improved without the need for a higher switching frequency. In particular, the harmonic component at the switching frequency $f_\mathrm{sw} = 10\,\mathrm{kHz}$ is significantly reduced from approximately $110\,\mathrm{V}$ to approximately $25\,\mathrm{V}$. The amplitude of the second harmonic of the switching frequency remains nearly unchanged at about $90\,\mathrm{V}$. Overall, the resulting total harmonic distortion (THD) decreases from approximately $8.8\,\%$ to $6.1\,\%$.

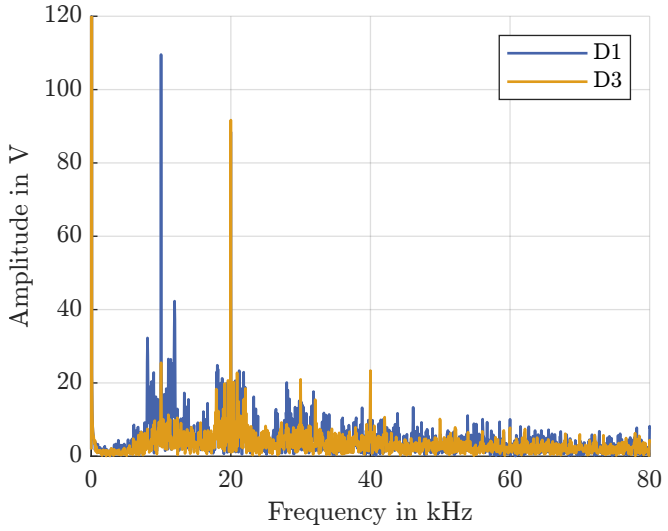

Fig. 12: Fourier spectrum of the line-to-line voltages $u_\mathrm{U} - u_\mathrm{V}$ with different module voltage distributions D1 (blue) and D3 (orange).

V. Conclusion

This paper presented a novel modulation scheme, referred to as FlexHex, for multilevel converters with distributed module voltages. By relaxing the constraint of equal module voltages, additional intermediate output levels can be synthesized, forming a multi-multilevel structure. This increases the resolution of available switching states and therefore reduces the VTAE without requiring higher switching frequencies.

Calculation results demonstrated that the proposed method reduces the maximum VTAE compared to conventional modulation techniques with uniform module voltages by up to $50\,\%$. Furthermore, the results show that the optimal module voltage distribution depends on the operating point of the converter. By appropriately adapting the module voltages, the VTAE can be reduced while maintaining the required output voltage capability, allowing an application-specific trade-off between modulation accuracy and voltage utilization.

In summary, FlexHex offers a flexible, albeit computationally intensive, method of improving the output voltage quality of modular multilevel converters. Future work will focus on experimental validation and on the implementation of dynamic voltage adaptation strategies to achieve real-time improvement of converter performance.

Acknowledgment

The authors gratefully acknowledge funding by the German Federal Ministry of Research, Technology and Space (BMFTR) within the Kopernikus Project ENSURE ‘New ENergy grid StructURes for the German Energiewende’.

References

[1] N. William McMurray Schenectady, “Fast response stepped wave switching power conversion circuit,” *United states patent 3,581,212*, vol. 1971, 1971.

[2] A. Nabae, I. Takahashi, and H. Akagi, “A New Neutral-Point-Clamped PWM Inverter,” *IEEE Transactions on Industry Applications*, vol. IA-17, no. 5, pp. 518–523, 1981.

[3] T. A. Meynard and H. Foch, "Multi-Level Choppers for High Voltage Applications," *EPE Journal*, vol. 2, no. 1, pp. 45–50, 1992. [Online]. Available: https://doi.org/10.1080/09398368.1992.11463285

[4] A. Lesnicar and R. Marquardt, "An innovative modular multilevel converter topology suitable for a wide power range," *2003 IEEE Bologna PowerTech - Conference Proceedings*, vol. 3, pp. 6–11, 2003.

[5] N. Menger, T. Merz, G. Zieglmaier, R. Schwendemann, and M. Hiller, "Decoupled Control Structure of a Modular Solid State Transformer," *2023 25th European Conference on Power Electronics and Applications, EPE 2023 ECCE Europe*, 2023.

[6] G. Pfaff, A. Weschta, and A. F. Wick, "Design and Experimental Results of a Brushless Ac Servo Drive," *IEEE Transactions on Industry Applications*, vol. IA-20, no. 4, pp. 814–821, 1984.

[7] H. C. Skudelny and G. V. Stanke, "Analysis and Realization of a Pulsewidth Modulator Based on Voltage Space Vectors," *IEEE Transactions on Industry Applications*, vol. 24, no. 1, pp. 142–150, 1988.

[8] S. Ogasawara, H. Akagi, and A. Nabae, "A novel PWM scheme of voltage source inverters based on space vector theory," vol. 74, pp. 33–41, 1990.

[9] J. Holtz, "Pulsewidth modulation - A survey," *PESC Record - IEEE Annual Power Electronics Specialists Conference*, vol. 049, no. 202, pp. 11–18, 1992.

[10] S. Kouro, P. Cortés, R. Vargas, U. Ammann, and J. Rodríguez, "Model predictive control - A simple and powerful Method to control power converters," *IEEE Transactions on Industrial Electronics*, vol. 56, no. 6, pp. 1826–1838, 2009.

[11] T. Geyer, N. Oikonomou, G. Papafotiou, and F. D. Kieferndorf, "Model predictive pulse pattern control," *IEEE Transactions on Industry Applications*, vol. 48, no. 2, pp. 663–676, 2012.

[12] J. Holtz, "Advanced PWM and Predictive Control-An Overview," *IEEE Transactions on Industrial Electronics*, vol. 63, no. 6, pp. 3837–3844, 2016.

[13] M. Schwenzer, M. Ay, T. Bergs, and D. Abel, "Review on model predictive control: an engineering perspective," *International Journal of Advanced Manufacturing Technology*, vol. 117, no. 5-6, pp. 1327–1349, 2021.

[14] M. Manjrekar and T. Lipo, "Hybrid multilevel inverter topology for drive applications," *Conference Proceedings - IEEE Applied Power Electronics Conference and Exposition - APEC*, vol. 2, pp. 523–529, 1998.

[15] A. Rufer, M. Veenstra, and K. Gopakumar, "Asymmetric multilevel converter for high resolution voltage phasor generation," *EPE 99 European Conference on Power Electronics and Applications*, 1999.

[16] M. Kuder, A. Kersten, L. Bergmann, R. Eckerle, F. Helling, and T. Weyh, "Exponential modular multilevel converter for low voltage applications," *2019 21st European Conference on Power Electronics and Applications, EPE 2019 ECCE Europe*, pp. P.1–P.11, 2019.

[17] T. Merz, N. Menger, F. Sommer, R. Schwendemann, and M. Hiller, "Continuous Sinusoidal Output Voltage Generation with a Single Phase Cascaded H-Bridge Converter," *2023 25th European Conference on Power Electronics and Applications, EPE 2023 ECCE Europe*, 2023.

[18] I. Trintis, S. Munk-Nielsen, and R. Teodorescu, "A new modular multilevel converter with integrated energy storage," *IECON Proceedings (Industrial Electronics Conference)*, pp. 1075–1080, 2011.

[19] N. Katzenburg, K. Kuhlmann, L. Leister, L. Stefanski, J. Teigelkotter, and M. Hiller, "Design of a Modular Multilevel Converter with 400 kWh of Integrated Batteries," *Proceedings of 22nd International Symposium on Power Electronics, Ee 2023*, 2023.

[20] B. Jacob and M. R. Baiju, "A new space vector modulation scheme for multilevel inverters which directly vector quantize the reference space vector," *IEEE Transactions on Industrial Electronics*, vol. 62, no. 1, pp. 88–95, jan 2015.

[21] R. C. Beltrame, M. L. Da Silva Martins, C. Rech, and H. L. Hey, "Hybrid power amplifiers - A review," *COBEP 2011 - 11th Brazilian Power Electronics Conference*, pp. 189–195, 2011.

[22] R. Schwendemann, M. Lorcher, F. Sommer, L. Stefanski, and M. Hiller, "A new, universal Series Hybrid Cascaded H-Bridge Converter for Power-Hardware in the Loop Emulation," *2019 21st European Conference on Power Electronics and Applications, EPE 2019 ECCE Europe*, 2019.